

Optimum Exchange for Calculation of Excitation Energies and Hyperpolarizabilities of Organic Electro-optic Chromophores

Kerry Garrett,[‡] Xochitl A. Sosa Vazquez,[†] Shawn B. Egri,[§] Jacob Wilmer,[†] Lewis E. Johnson,[‡] Bruce H. Robinson,[‡] and Christine M. Isborn^{*,†}

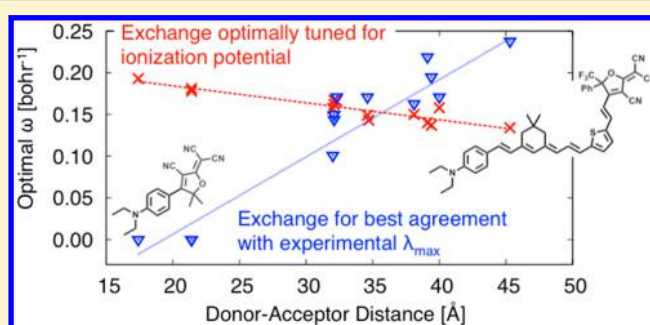
[†]Chemistry and Chemical Biology, University of California Merced, Merced, California 95343, United States

[‡]Department of Chemistry, University of Washington, Seattle, Washington 98195, United States

[§]Department of Chemistry, University of Vermont, Burlington, Vermont 05405, United States

S Supporting Information

ABSTRACT: Organic electro-optic (OEO) materials integrated into silicon–organic hybrid devices afford significant improvements in size, weight, power, and bandwidth performance of integrated electronic/photonics systems critical for current and next generation telecommunication, computer, sensor, transportation, and defense technologies. Improvement in molecular first hyperpolarizability (β), and in turn electro-optic activity, is crucial to optimizing device performance. Common hybrid density functional theory (DFT) methods, while attractive due to their computational scaling, often perform poorly for optical properties in systems with substantial intramolecular charge-transfer character, such as OEO chromophores. This study evaluates the utility of the long-range corrected (LC) DFT methods for computation of the molecular second-order nonlinear optical response. We compare calculated results for a 14-molecule benchmark set of OEO chromophores with the corresponding experimentally measured β and one-photon absorption energy, λ_{max} . We analyze the distance dependence of the fraction of exact exchange in LC-DFT methods for accurately computing these properties for OEO chromophores. We also examine systematic tuning of the range-separation parameter to enforce Koopmans' ionization potential theorem. This tuning method improves prediction of excitation energies but is not reliable for predicting the hyperpolarizabilities of larger chromophores since the tuning parameter value can be too small, leading to instabilities in the computation of β_{HRS} . Additionally, we find that the size dependence of the optimal tuning parameter for the ionization potential has the opposite size dependence of optimal tuning parameter for best agreement with the experimental λ_{max} suggesting the tuning for the ionization potential is unreliable for extended conjugated systems.



1. INTRODUCTION

Electro-optic materials are critical for current and next generation sensor technology such as nano- and microantennae elements central to wireless communication. The integration of organic electro-optic (OEO) materials into silicon photonic waveguide devices has led to state-of-the-art defining bandwidth, drive voltage, and power efficiency.^{1–4} Improvement in each of these properties has been made possible by improvement in the electro-optic activity of the materials used in these devices. Drive voltage and power efficiency of devices is defined by EO activity, which is in turn proportional to chromophore molecular first hyperpolarizability, β , a measure of the extent to which a molecule asymmetrically polarizes in response to an applied electric field.^{5–8}

For an organic molecule, β is maximized in donor– π –acceptor (D– π –A) structures. In these systems, a π -conjugated bridge connects an electron-donating (D) group with an electron-withdrawing (or accepting, A) group on either end of the (typically linear) chromophore. Increasing the strength of

the donor or acceptor or the length of the bridge usually leads to larger hyperpolarizability component (β_{zzz}) along the dipole axis, which we will define as the z -axis in the frame of the molecule. One of the most successful strong acceptor moieties is tricyanofuran (TCF), commonly linked through a π -conjugated thienylenevinylene (FTC-type) or polyene (CLD-type) bridge to a substituted aniline donor.⁹ However, due to centrosymmetric pairing between the strong dipoles of these systems, they tend to exhibit limited poling-induced ordering at a high density, a necessary condition for the bulk EO response.^{5,10} In order to overcome these limitations while maintaining or improving β_{zzz} values, there is a continued effort to synthesize new donor and acceptor pairs, as well as to study how these end groups communicate through different π -conjugated linkers.¹¹ Due to the cost in time and materials to explore various synthetic routes, theoretical tools have become

Received: June 18, 2014

Published: August 15, 2014

increasingly useful for developing structure–property relations for OEO materials.¹²

To rationally design better OEO materials with theory as a guide, it is necessary to develop a computational method that can reliably predict the electronic properties of interest for a variety of donor, acceptor, and bridge combinations. Because the molecular hyperpolarizability is a frequency dependent property, an ideal computational method should be able to accurately predict both optical transitions and the hyperpolarizability. Density functional theory (DFT) is the method of choice for many organic molecules, including large conjugated systems such as those studied in this work, due to its favorable accuracy/cost ratio. Furthermore, the development of time-dependent density functional theory (TDDFT) has made it possible to theoretically predict excited state properties of large molecules.¹³ Many useful optical properties such as the peak one-photon absorption energy, λ_{max} , excited state dipole moments, μ_{ex} , and static and dynamic polarizabilities and hyperpolarizabilities, can be calculated using TDDFT.

Although both DFT and TDDFT are exact theories, using standard approximate exchange–correlation functionals leads to a few well-known limitations. Due to the overdelocalization error, also known as self-interaction error, which comes from using an approximate form of the exchange interaction, DFT is known to overestimate polarization, underestimate bandgaps, and underestimate reaction barrier heights.^{14–20} TDDFT typically overestimates Rydberg excitation energies²¹ and poorly reproduces charge-transfer excitation energies.¹³ This latter phenomenon is due to the lack of proper Coulombic 1/*R* attraction between the excited electron and hole. This is a consequence of the short-range treatment of exchange in typical LSDA/GGA functionals, as opposed to the exact exchange used in the Hartree–Fock method. The lack of exact exchange in typical DFT functionals often leads to severe underestimation of charge-transfer energies. This issue is of great consequence for D- π -A systems that are expected to have significant charge-transfer character.²²

The addition of some exact exchange to a functional, replacing a fraction of the short-range LSDA/GGA exchange, generally helps alleviate both the DFT overdelocalization error (since full exact exchange without nonlocal correlation as in Hartree–Fock theory leads to the opposite effect, giving an overlocalization error) and the TDDFT charge-transfer excitation energies.^{16,23–31} The incorporation of exact exchange can be performed through either a hybrid functional, which uses a fixed amount of exchange at all interelectronic distances, or a long-range corrected (LC) functional, which uses a larger fraction of exact exchange (often 100%) at long-range interelectronic distances and a larger fraction of LSDA/GGA DFT exchange at short-range.^{21,32,33} For LC functionals, the scaling between the long-range and short-range is determined by the tunable parameter ω , sometimes also denoted by γ or μ , defined in units of inverse length (a_0^{-1} , bohr⁻¹). Larger values of ω lead to a larger percentage of exact exchange for a given interelectronic distance.

The delocalization error of pure DFT functionals generally leads to larger predicted dipole moments and polarizabilities compared to methods with exact exchange.^{28,34–40} Because each molecule exhibits different degrees of the delocalization error,^{41,42} it is appealing to look to a system specific procedure for determining the appropriate amount of exact exchange to minimize the error. This can be accomplished by tuning ω to enforce a particular physical property. One popular ω -tuning

procedure is to use the amount of exact exchange at which the energy of the ionization potential (IP) matches the energy of the highest occupied molecular orbital. This procedure, pioneered by Baer, Kronik, and co-workers,^{31,43–46} has been shown to yield improved band gap energies and excitation energies.^{22,47–49} However, recent work by Champagne and co-workers has shown that ω -tuning for the IP leads to large overestimates of the polarizability and second hyperpolarizability (γ) for large π -conjugated systems when compared to more accurate coupled-cluster results.⁴⁰ This is in contrast to work by Sun and Autschbach which shows that IP ω -tuning leads to fairly mild overestimation of the first hyperpolarizability β compared to Møller–Plesset second-order perturbation (MP2) calculations.⁵⁰

In this work, we examine the effects of the range-separation parameter on the accuracy of the computed excitation energy and first hyperpolarizability β compared to experimental values for a benchmark set of 14 nonlinear optical (NLO) charge-transfer chromophores. Calculations were run using three different LC density functionals. We use these calculations as a benchmark to determine if tuning of ω improves the accuracy of these computed properties. In section 2, we describe the commonly used ω -tuning procedure based on Koopmans' theorem. In section 3, we give details on the benchmark test set along with summarizing the corresponding experimental results. Section 4 includes computational details, such as a discussion of computing the hyperpolarizability β and comparing to experimentally measurable values. In section 5, we present our results of tuning ω values, along with computing the excitation energies and hyperpolarizabilities at various ω values.

2. ω -TUNING

Long-range correction schemes use a pair of complementary, continuous functions (most commonly the error function) to partition the interelectronic distance, $r_{12} = |\mathbf{r}_1 - \mathbf{r}_2|$, between long-range (LR) and short-range (SR) terms (eq 1):

$$\frac{1}{r_{12}} = \frac{1}{r_{12}}[\text{erf}(\omega r_{12})] + \frac{1}{r_{12}}\{1 - [\text{erf}(\omega r_{12})]\} \quad (1)$$

where ω is the range-separation parameter, with larger values of ω increasing the contribution from the long-range term. Setting $\omega = 0$ removes all contribution from the long-range term at all r_{12} distances. The long and short-range components replace the interelectronic distance for short-range LSDA/GGA exchange and long-range exact (Hartree–Fock) exchange, respectively (eq 2).

$$E_x = E_x^{\text{LR,exact}} \left(\frac{1}{r_{12}}[\text{erf}(\omega r_{12})] \right) + E_x^{\text{SR,DFT}} \left(\frac{1}{r_{12}} \{1 - [\text{erf}(\omega r_{12})]\} \right) \quad (2)$$

The default values for ω in LC-BLYP and LC- ω PBE, two of the functionals used in this work, are 0.47 and 0.40 bohr⁻¹, respectively. In both functionals, 100% exact exchange is used at infinite distance, and no exact exchange is used at zero distance. The third functional, CAM-B3LYP, has a more complex functional form that introduces additional parameters to specify the fraction of exact exchange used at the zero and infinite-distance limits. In CAM-B3LYP, the ω parameter adjusts the amount of exact exchange between default values of

65% at long-range to 20% at short-range, with a default ω value of 0.33 bohr^{-1} .²¹

The optimal range-separation parameter, ω , has been found to be highly system-dependent. Several strategies have been developed to combat this issue, such that ω can be chosen in a “system-specific but non-empirical way.”⁵¹ These tuning strategies are based on a choice of ω that satisfies a known property. One property that the true, exact density functional should possess is that the computed ionization potential (IP = $E(N) - E(N - 1)$, where N is the number of electrons in the molecule) of a molecule should be equal to the negative of the energy of the highest occupied molecular orbital, ϵ_{HOMO} , that is, it should obey Koopmans’ theorem.⁴⁵ The optimum ω is then determined by finding when the following function is closest to zero

$$\Delta_{\text{IP}}(\omega) = E_{\text{HOMO}}(\omega, N) - [E(\omega, N) - E(\omega, N - 1)] \quad (3)$$

For charge-transfer chromophores, ω can also be tuned based on the electron affinity (EA). This can be done by enforcing agreement between the energy of the lowest unoccupied molecular orbital (LUMO) and the EA by finding when the following is closest to zero²²

$$\Delta_{\text{EA}}(\omega) = E_{\text{LUMO}}(\omega, N) - [E(\omega, N) - E(\omega, N + 1)] \quad (4)$$

or by tuning ω to enforce Koopmans’ theorem for the anion

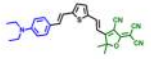
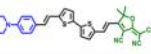
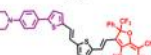
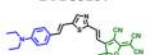
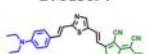
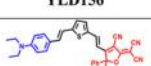
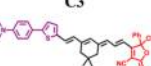
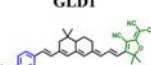
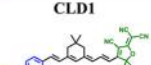
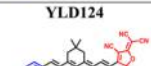
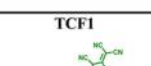


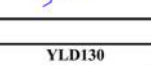
$$\Delta_{\text{IP}}(\omega) = E_{\text{HOMO}}(\omega, N + 1) - [E(\omega, N + 1) - E(\omega, N)] \quad (5)$$

By “tuning” ω in an LC functional to the value at which the IP = $-\epsilon_{\text{HOMO}}$, the delocalization error can be minimized, which has been shown to improve the accuracy of some computed molecular properties, such as IP, EA, fundamental energy gaps, and optical absorption spectra.^{22,52} We characterize these methods for a series of chromophores for both excitation energies and hyperpolarizability.

3. BENCHMARKS AND EXPERIMENTAL RESULTS

Structures and experimental properties for the 14-molecule test set are shown in Table 1. Each of the molecules in this test set possesses a similar structural motif: a tricyanofuran (TCF) acceptor is linked through a π -conjugated bridge to an N,N -diethylaniline donor. There are two different donors, the standard N,N -diethyl-aniline donor and the diethyl-amino-phenyl-thienyl (APT) donor, and three different acceptors, the standard dimethyl-TCF acceptor, the CF_3 -phenyl-substituted TCF acceptor, and the CF_3 -substituted TCF acceptor (color coded in Table 1). The 14 chromophores were classified according to their bridge structure as either FTC-type (thienylenevinylene bridge), CLD-type (polyene bridge),⁹ “hybrid” (in the case of YLD130), or “short-bridge” if they contain less than one vinylene unit in the bridge. The donor–acceptor (D-A) length of each of the chromophores according to the distance between the nitrogen (N) atom on the diethyl-aniline donor and the malononitrile carbon (C) atom of the TCF acceptor, as shown in Figure 1, was determined from the optimized geometry (details given in section 4). The λ_{max} in Table 1 is from the UV–vis absorption spectrum of the chromophores in chloroform. Available spectra are given in the Supporting Information (SI), Figure S1.

Table 1. Nonlinear Optical Chromophore Structure, Computed Donor–Acceptor Length, Experimental λ_{max} , and Experimental Relative First-Order Hyperpolarizabilities, $\beta_{\text{HRS}}^{\text{sys}}/\beta_{\text{HRS}}^{\text{EZFTC}}$, Measured in CHCl_3 ^a

Name and Structure ^b	D-A length, calculated (Å)	Experimental λ_{max} in CHCl_3 (nm, eV)	Experimental $\beta_{\text{HRS}}^{\text{sys}}/\beta_{\text{HRS}}^{\text{EZFTC}}$ at 1907 nm in CHCl_3 ^c
EZFTC (Reference) 	32.1	676, 1.83	1.0
FTC-type systems			
OLD3 	40.0	677, 1.83	1.4
C2 	38.1	746, 1.66	2.8*
DMC3257 	32.3	682, 1.82	1.1
DMC3194 	32.1	645, 1.92	0.76
YLD156 	32.0	754, 1.64	2.1*
CLD-type systems			
C3 	39.4	777, 1.60	5.7*
GLD1 	39.1	719, 1.72	3.0
CLD1 	34.6	691, 1.79	1.8*
YLD124 	34.7	786, 1.58	5.4*
Short-bridge systems			
TCF1 	21.4	587, 2.11	0.33*
TCF1_CF3 	21.4	629, 1.97	0.36*
DCDHF 	17.4	493, 2.52	Not available
Hybrid CLD-FTC bridge			
YLD130 	45.3	817, 1.52	Not available

^aIn addition to classifying the bridge character as FTC-type, CLD-type, or short-bridge, we also classify the donor (D) and acceptor (A) moieties with color-coding. The standard N,N -diethyl-aniline donor is colored in blue; the standard TCF acceptor is colored in green; the

Table 1. continued

diethyl-amino-phenyl-thienyl (APT) donor is colored in purple; and the CF₃-phenyl-substituted TCF acceptor is colored in red. The TCF1_CF3 chromophore has a CF₃-substituted TCF acceptor that is highlighted in orange. ^bDMC3 systems were synthesized by Daniel Casmier; YLD systems by Yi Lao; CLD1 by Yen-Ju Cheng; EZFTC and OLD3 by Olivier Clot; TCF1 systems by Sei-Hum Jang; DCDHF by Peter Johnston; C2,C3 systems by Andrew Akelaitis; and GLD1 was synthesized at University of Southern California. ^cHRS measurements were performed by Kim Firestone and David Lao, unless noted by an asterisk (*) for measurements performed by Denise Bale.⁷

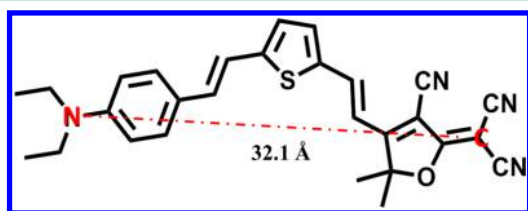


Figure 1. EZFTC chromophore. Distance between donor nitrogen (highlighted 'N') and malononitrile carbon (highlighted 'C') of the acceptor as a metric of the chromophore length, labeled D-A length in Table 1.

The last column of Table 1, labeled as $\beta_{\text{HRS}}^{\text{sys}}/\beta_{\text{HRS}}^{\text{EZFTC}}$, reports the hyperpolarizability measured with hyper-Rayleigh scattering (HRS) and taken as a ratio with respect to the reference solution of EZFTC in chloroform. All experimental HRS values were measured in chloroform at 1907 nm and using EZFTC as an external reference.^{7,53,54} Reporting these values as a ratio facilitates comparison with hyperpolarizability data from other works, which can be reported using three different conventions for magnitude.⁵⁵ Although $\beta_{\text{HRS}}(-2\omega, \omega, \omega)$ is not the true figure-of-merit for an electro-optic material, HRS measurements are the most common method of quantifying β experimentally. More important is the principal element of the β tensor, β_{zzz} , coincident with the molecular symmetry/dipole axis (by convention, the z-axis). β_{zzz} makes the largest contribution to the averaged β , such that $\beta_{\text{HRS}}(-2\omega, \omega, \omega) \approx \sqrt{(6/35)}\beta_{\text{zzz}}(-2\omega, \omega, \omega)$, for a given frequency or solvent.^{6,7,56} Here, we include the full averaging over all β tensor components for computation of β_{HRS} . Comparison of the experimental and computed β_{HRS} is complicated by the issue of resonant enhancement in both calculations and experiment and two-photon fluorescence (TPF) interference effects in the HRS experiment.⁸ These effects result in an increase in measured β_{HRS} due to absorption near the second harmonic. By using 1907 nm excitation, both the input frequency and the second harmonic are far from the absorption bands of most of the chromophores in this test set, minimizing resonant enhancement and TPF effects. Two of the chromophores, YLD124 and C3, have nontrivial absorbance near 950 nm, the second harmonic frequency of the laser, which likely leads to some enhancement in the experimental β_{HRS} value; indeed, the β_{HRS} ratios for these two chromophores (ratios of 5.4 and 5.7, respectively) are significantly larger than the other chromophores in this test set (β_{HRS} ratios ranging 0.36–3).

4. COMPUTATIONAL DETAILS

All electronic structure calculations were performed with the Gaussian 09 Rev. D.01 software package.⁵⁷ The geometries of

the molecules were optimized at the B3LYP/6-31+G* level of theory using an “ultrafine” integration grid (99 radial and 590 angular points per shell) and default convergence settings, using a RMS force criterion of 3×10^{-4} au or less. For comparison with experimental measurements, calculations were run in a chloroform solvent environment ($\epsilon = 4.7113$) using default polarizable continuum model (PCM) settings. The PCM environment was used for all geometry optimizations. The solvent-optimized geometry of the neutral molecule was used for all open- and closed-shell energy calculations necessary for ω -tuning, which were run in both vacuum and PCM environments. Vacuum calculations are noted in the text. Nonequilibrium excited-state solvation was employed for all TDDFT calculations. For TDDFT calculations, the excitation energy of the state with the largest oscillator strength was compared to the experimental λ_{max} . Properties and ω -tuning were computed with the LC-BLYP, LC- ω PBE, and CAM-B3LYP density functionals.^{21,33,58} A previous benchmarking study has shown that for LC- ω PBE excitation energies, an ω value of 0.2 bohr⁻¹ gives better agreement with experiment.^{59,60} LC-BLYP results are presented in the main document, while LC- ω PBE and CAM-B3LYP results are given in SI.

The frequency-dependent hyperpolarizabilities consistent with HRS measurements, $\beta_{\text{HRS}}(-2\omega, \omega, \omega)$, were computed at 1907 nm from analytical derivatives of the energy with respect to field strength obtained via the coupled-perturbed Kohn–Sham (CPKS) method.⁶¹ No calculations of the hyperpolarizability are presented for LC- ω PBE because of the lack of analytical third derivatives for this functional in the Gaussian program. Results are generally quite similar for LC-BLYP and ω PBE for ω -tuning and excitation energy trends (sections 5.1 and 5.2, respectively); therefore, they are likely to behave similarly for the computed hyperpolarizability. Frequency-dependent hyperpolarizabilities can become drastically inflated near an optical resonance, in this case, when an excitation overlaps with laser frequency of 1907 nm or its second harmonic of 953 nm. Therefore, calculations of static hyperpolarizabilities are generally more indicative of how structure affects the NLO character of these systems and thus can be more useful than the frequency-dependent quantities; we therefore also report the static hyperpolarizability for β_{zzz} , the component of the hyperpolarizability tensor along the dipole moment of the chromophore. While the Gaussian program reports hyperpolarizabilities in the Taylor expansion convention, our values are reported with the perturbation convention, which involves dividing the Taylor expansion convention values by two.⁵⁵ These varying conventions are another reason to compare the ratios of hyperpolarizabilities rather than unscaled values.

Conformational Analysis. Previous conformational analysis studies based on FTC and CLD structures have suggested that several rotamers of these chromophores can coexist in low-viscosity solution.^{9,11} The prototype FTC and CLD conjugated bridges, EZFTC and CLD1, as shown in Figure 2, contain three rotatable single bonds that can exist in the cisoid (c) or transoid (t) conformation resulting in eight possible conformers: *ttt*, *ttc*, *ctt*, *ctc*, *tct*, *tcc*, *cct*, and *ccc*. The geometries of the eight conformers were optimized and the resulting structures used to compute the excitation energy and hyperpolarizability (see Table S1 in the SI). The reported energies are computed at the PCM-B3LYP/6-31+G* level of theory, while the properties are computed with PCM-LC-BLYP/6-31+G* with the default range tuning parameter of $\omega = 0.47$ bohr⁻¹.

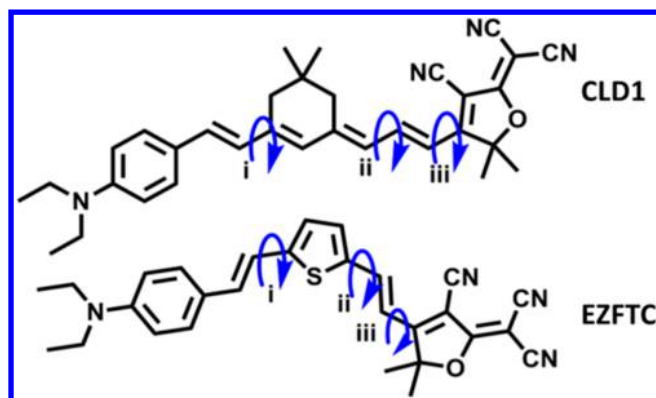


Figure 2. CLD1 and EZFTC molecules in trans–trans–cis (*ttc*) configuration. Three rotatable bonds are labeled i, ii, iii.

The Boltzmann populations at 298 K, labeled as statistical weights, reveal that only the *ttc* and *ttt* conformers of CLD1 have a probability above 1%. For these two conformers, the computed properties of interest are quite similar; the respective dipole moments vary minimally from 24.1 to 25.2 D, the excitation energies are 2.01 and 2.03 eV, $\beta_{\text{HRS}}(0)$ varies slightly from 193×10^{-30} to 205×10^{-30} esu, and the difference in $\beta_{\text{zzz}}(0)$ is similarly negligible. For chromophores in the benchmarking set with the CLD-type bridge (CLD1, GLD1, YLD124, and C3), we use the *ttc* conformer for all subsequent computation. For EZFTC, the *ttt* and *ttc* conformers are also the most likely (37% and 34% statistical weights, respectively), while the *ctc* and *ctt* conformers both have weights of 11%. For the two dominant conformers, the excitation energy and β_{HRS} values are quite similar; however, upon rotation of the TCF group from transoid to cisoid, the computed dipole moment increases by ~ 3 D and the $\beta_{\text{zzz}}(0)$ value also increases. The static hyperpolarizability varies substantially for the four conformers: $\beta_{\text{zzz}}(0)$ nearly doubles from 167×10^{-30} esu for *ctt* to 291×10^{-30} esu for *ttc* and *ctc*. Since β_{HRS} is computed as an orientational average of the tensor components of β , it is not surprising that $\beta_{\text{HRS}}(0)$ varies less than the single tensor component $\beta_{\text{zzz}}(0)$ which is aligned in the direction of the dipole (*z*-) axis. Although not the lowest energy conformer, for consistency with the CLD-type structures, we have chosen to use the *ttc* conformer for the FTC-type structures (EZFTC, YLD156, OLD3, DMC3194, DMC3257, and C2). Also, we use the *ttc* (transoid-bridge, cisoid TCF) geometry for the short-bridge systems (DCDHF, TCF1, TCF1_CF3) as well as the hybrid system, YLD130.

5. RESULTS AND DISCUSSION

5.1. Optimum ω for Enforcing Koopmans' Theorem.

Tuning ω such that the HOMO energy is consistent with Koopmans' theorem indicated a general correlation between molecular length and optimal ω value for each of the functionals used. LC-BLYP vacuum results are shown in Figure 3, LC- ω PBE and CAM-B3LYP vacuum results are in SI Figures S2 and S3, respectively. The optimum ω value occurs when the energy difference is zero (on the *x*-axis). Chromophores are specified by a ROYGBV color scheme that roughly corresponds to their D-A length (given in Table 1). Longer chromophores are colored red, shorter chromophores are colored purple. For most chromophores, the longer the conjugation length of the bridge, the more the optimal ω shifts closer to zero. This trend has been previously reported by Baer, Brédas, and

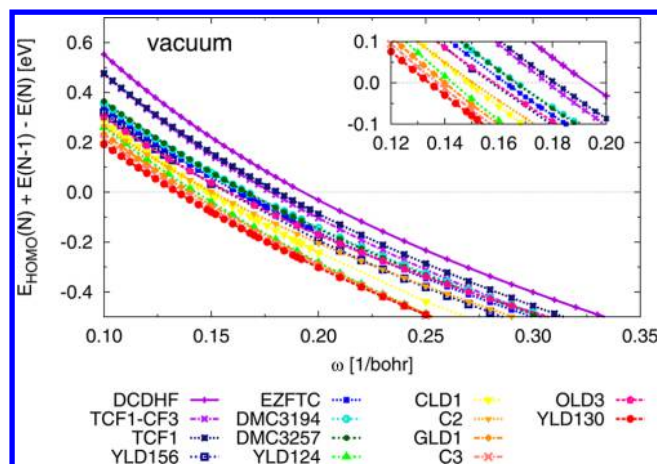


Figure 3. LC-BLYP vacuum ω -tuning for Koopmans' theorem. The ionization potential matches the HOMO energy at the *x*-axis. Chromophore size (roughly indicated by color) generally yields a larger ω value for smaller chromophores ($\omega = 0.18$ – 0.19 bohr $^{-1}$) and smaller ω value for larger chromophores ($\omega = 0.13$ – 0.14 bohr $^{-1}$). For larger values of ω , the HOMO energy is larger in magnitude than the ionization potential.

others.^{22,40,43,45,49,50,62,63} The optimal ω for LC-BLYP in vacuum ranges from 0.13 bohr $^{-1}$ to 0.19 bohr $^{-1}$, where smaller chromophores have the larger optimal ω and the larger chromophores have the smallest ω values. A similar range is observed in LC- ω PBE. Although the CAM-B3LYP range is larger than that of LC-BLYP or LC- ω PBE (0.28 bohr $^{-1}$ to 0.62 bohr $^{-1}$), it follows the same chromophore size trend.

Comparison of four CLD-type systems which have identical donor (*N,N*-diethyl-aniline) and acceptor (TCF) units but varying conjugation length (*n* units) of the polyene bridge, namely DCDHF ($n = 0$), TCF1 ($n = 1$, monoene), CLD1 ($n = 4$, tetraene), and GLD1 ($n = 5$, pentaene), clearly displays this trend in optimal ω . The OLD3 chromophore contains the same donor and acceptor groups, but they are bridged by adjacent thiophenes. This chromophore behaves as an outlier with the D-A length trends since its ω -tuning value is more in line with that for a smaller chromophore. The addition of the phenyl and CF $_3$ groups to the TCF acceptor does not affect the D-A length according to our distance metric but does lead to a smaller optimal ω value, suggesting that perhaps total number of electrons could correlate with optimal ω trends better than D-A length. Indeed, a linear least-squares fit of optimum ω value to chromophore D-A length gives $R^2 = 0.85$, while a linear fit of optimum ω value to chromophore number of electrons gives $R^2 = 0.87$.

When the PCM environment is included in the ω -tuning calculations, the optimum ω values are shifted by approximately 0.1 bohr $^{-1}$ smaller than in vacuum for LC-BLYP and LC- ω PBE (see LC-BLYP PCM results in Figure 4, LC- ω PBE and CAM-B3LYP PCM results in SI Figures S4 and S5). The trends in chromophore size are similar to vacuum, with a larger ω value for smaller chromophores ($\omega \approx 0.045$ bohr $^{-1}$) and smaller ω value for larger chromophores ($\omega \approx 0.03$ bohr $^{-1}$). The CAM-B3LYP ω trends are the same but with a greater change than LC-BLYP and LC- ω PBE. Whereas the LC-BLYP largest optimal ω changed from ≈ 0.19 bohr $^{-1}$ in vacuum to ≈ 0.05 bohr $^{-1}$ in PCM, CAM-B3LYP changed more drastically from ≈ 0.62 bohr $^{-1}$ in vacuum to ≈ 0.02 bohr $^{-1}$ in PCM. The shift in ω value suggests that the PCM environment may dominate the

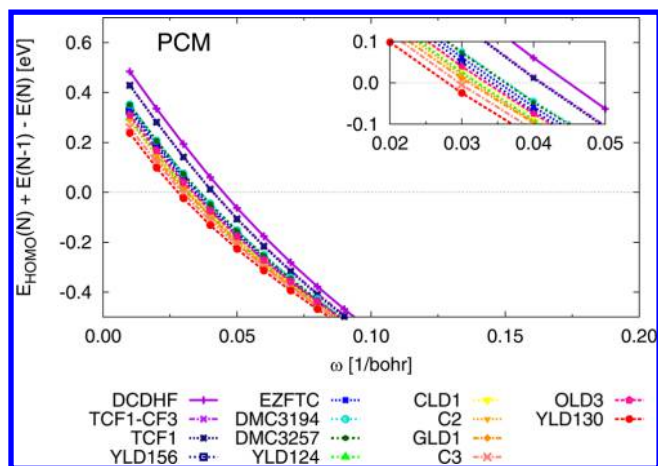


Figure 4. LC-BLYP PCM ω -tuning for Koopmans' theorem. The ionization potential matches the HOMO energy at the x -axis. Chromophore size trends generally predict a larger ω value for smaller chromophores ($\omega = 0.045 \text{ bohr}^{-1}$) and smaller ω value for larger chromophores ($\omega = 0.03 \text{ bohr}^{-1}$). While the trends in chromophore size are similar to vacuum, the PCM optimum ω values are approximately 0.1 bohr^{-1} smaller than in vacuum.

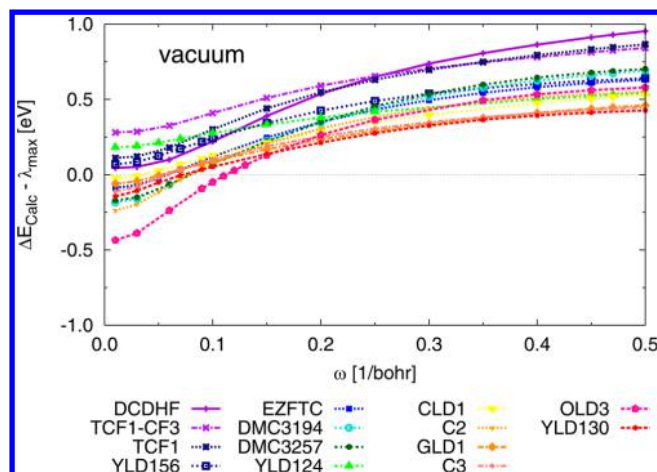


Figure 5. Difference in vacuum TD-LC-BLYP computed transition energy ΔE_{Calc} and experimental λ_{max} in CHCl_3 . For larger values of ω , the computed transition energy is overestimated. Chromophore size trends generally predict that a more accurate excitation energy is computed with a larger ω value for larger chromophores (0.10 bohr^{-1}) and smaller ω value for smaller chromophores (0.0 bohr^{-1} , a "pure" DFT functional).

energy of the cation species involved in ω -tuning. This will be explored further in future work.

For LC-BLYP and LC- ω PBE in both the vacuum and PCM environments, the trends based on the electron affinity and the HOMO energy of the anion (eq 5) and the optimum ω values are very similar to those just discussed for ω -tuning for the ionization potential of the neutral chromophore (see SI Figures S6–S11). With CAM-B3LYP in vacuum, ω -tuning for the ionization potential of the anionic chromophore gives large ω values than ω -tuning for the ionization potential of the neutral chromophore. The short-range exact exchange included in CAM-B3LYP may lead to a different treatment of the anion. We also examined the ω -tuning results for the LUMO energy of the neutral chromophore matching the electron affinity (eq 4) and once again found nearly identical trends and ω values.

5.2. Optimum ω for Electronic Excitation Energies.

We next examine how the value of ω affects the excitation energy and if the ω tuned for Koopmans' theorem provides more accurate results when comparing with the experimental λ_{max} . The results for LC-BLYP with TDDFT excitation energies computed in vacuum are shown in Figure 5 (SI Figures S12 and S13 give comparable results for LC- ω PBE and CAM-B3LYP). The difference is taken between the computed bright state excitation energy and the experimental λ_{max} in solution. At large ω values with larger amounts of exact exchange, the excitation energy is overestimated, with the excitation energy decreasing as the ω value decreases. This is aligned with the previously observed trend of CIS and time-dependent Hartree–Fock (TDHF) calculations overestimating charge-transfer excitation energies and TDDFT with pure GGA functionals often underestimating excitation energies.^{13,60,64,65} Better agreement with the experimental λ_{max} is seen with ω values between 0 and 0.1 bohr^{-1} . These values are much smaller than the default ω value of 0.47 bohr^{-1} , and slightly smaller than those obtained from the ω -tuning for Koopman's theorem in vacuum. This means that the excitation energy would be overestimated if using the ω values obtained by optimizing for Koopman's theorem in vacuum, by up to $\sim 0.5 \text{ eV}$.

As with the ω -tuning for Koopman's theorem, there is a clear trend with chromophore size. However, the trend is *opposite* that predicted by enforcing Koopman's theorem: a more accurate excitation energy is computed with larger ω values for larger molecules, and smaller ω values for smaller molecules. Thus, while using the ω value tuned for Koopman's theorem will give a value in better agreement with experiment than the default ω value, the trend with molecular size would be incorrect. This suggests an underlying problem with ω -tuning for Koopman's theorem with molecules of different size.

Similar trends are observed with the PCM environment included in the excited state computation (see Figure 6). The inclusion of the solvent environment lowers the computed excitation energy for all chromophores. This shift leads to larger

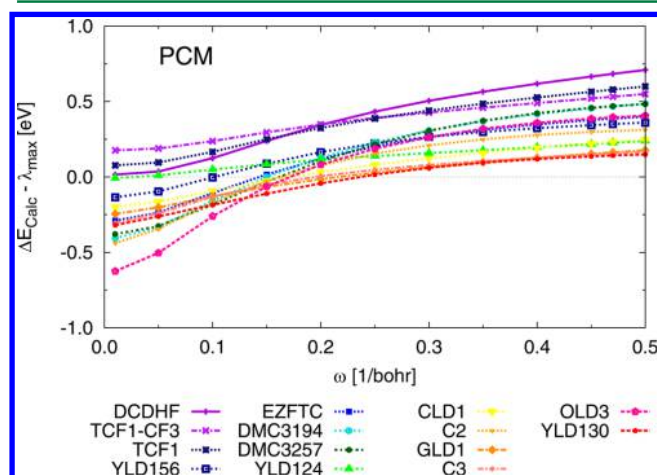


Figure 6. Difference in PCM TD-LC-BLYP computed transition energy ΔE_{Calc} and experimental λ_{max} in CHCl_3 . The PCM environment lowers the excitation energy for all chromophores by 0.1 – 0.3 eV . Chromophore size trends are similar to vacuum, generally predicting that a more accurate excitation energy is computed with a larger ω value for larger chromophores (0.25 bohr^{-1}) and smaller ω value for smaller chromophores (0.0 bohr^{-1}).

optimum ω values for obtaining the best agreement with λ_{\max} with the optimum ω range being 0–0.25 bohr⁻¹. This is in direct contrast to ω -tuning for Koopman's theorem with PCM, which predicts smaller optimum ω values compared to vacuum. Even with the PCM environment, the excitation energy is overestimated at all values of ω for the smallest chromophores. For most of the test set, the excitation energy would be underestimated by up to ~0.5 eV if using the small ω values obtained by optimizing for Koopman's theorem in PCM. Because of the better agreement when using PCM with the default ω value, optimal ω -tuning for Koopman's theorem with PCM would give less accurate excitation energies for a number of chromophores in this test set.

The opposite trends in chromophore size when ω -tuning for Koopman's theorem vs excitation energy for both vacuum and PCM environments are shown in Figure 7 (SI Table S2 gives

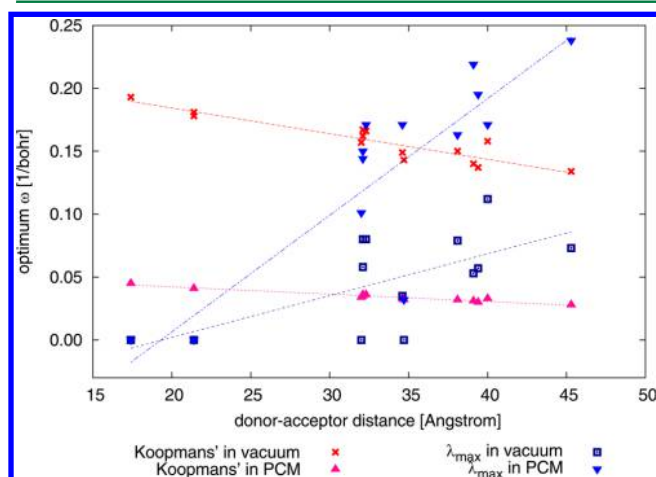


Figure 7. Correlation of optimum ω value (by agreement with Koopman's theorem or experimental λ_{\max}) with distance between donor and acceptor group on the chromophore. Oppositely signed slopes are observed for Koopman's theorem and experimental λ_{\max} optimum ω values. The straight lines are linear regression fits to guide the eye.

the optimal ω values for each functional). Agreement with Koopman's theorem shows a fairly linear trend that the optimum ω should decrease with increasing chromophore size. Choosing the optimum ω value that yields the best agreement with λ_{\max} shows that the optimum ω should increase with increasing chromophore size, (i.e., that more exchange is necessary for accurately describing the excitation energies of larger OEO chromophores). The opposite trend for best agreement with experiment and ω -tuning for Koopman's theorem points to the possibility of overtuning for large molecular systems (i.e., that the delocalization error of DFT may lead to size-related inconsistencies in describing the ionization potential or energy of the HOMO). This effect will be explored in future studies.

5.3. Optimum ω for Hyperpolarizabilities. In this section, we probe the effect of ω on the computed hyperpolarizabilities. Figure 8 shows the PCM/LC-BLYP/6-31+G* computed static β_{zzz} values as a function of ω . As expected, chromophores with longer D-A bridges generally yield larger β_{zzz} values. While β_{zzz} clearly increases with decreasing exact exchange for some chromophores (most notably YLD130 and OLD3), for other chromophores there is a leveling off or decrease in β_{zzz} with small range separation

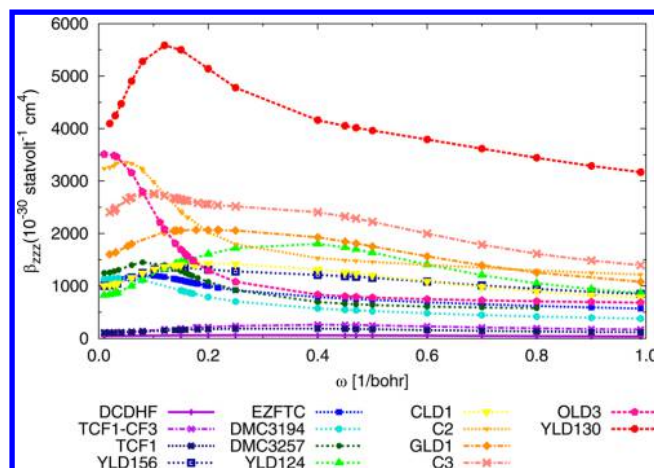


Figure 8. Computed LC-BLYP/6-31+G* static hyperpolarizability aligned with the dipole axis, β_{zzz} in esu (10^{-30} statvolt⁻¹ cm⁴).

parameters ($\omega < 0.2$ bohr⁻¹). There is not as clear of a trend with β_{zzz} value and ω as is seen with other properties.

Because the experimental β_{HRS} value is reported as a ratio with respect to the EZFTC molecule, we compared the same ratio for our plots of the computed β_{HRS} values. The unscaled β_{HRS} values are given in SI Figure S16 and Table S3. The ratios for static β_{zzz} and frequency dependent β_{HRS} are shown in Figure 9 for LC-BLYP and in SI Figure S17 for CAM-B3LYP.

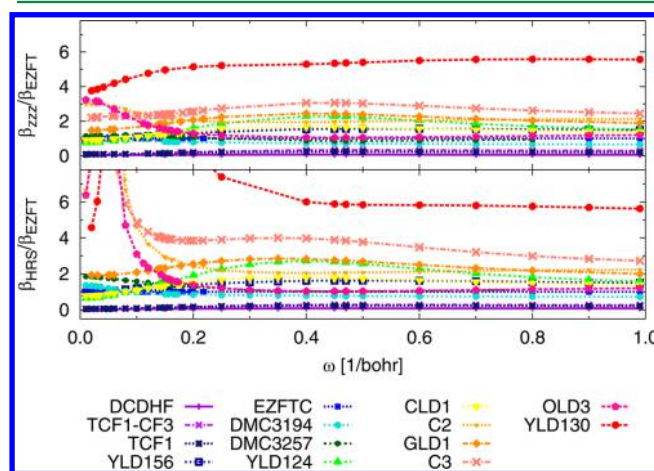


Figure 9. (Top) Computed LC-BLYP static hyperpolarizability aligned with the dipole axis, $\beta_{zzz}/\beta_{zzz}^{\text{EZFTC}}$. (Bottom) Computed LC-BLYP frequency-dependent hyperpolarizability, $\beta_{\text{HRS}}(-2\omega; \omega, \omega)/\beta_{\text{HRS}}^{\text{EZFTC}}$ at 1906 nm. Trends are similar for $\beta_{zzz}/\beta_{zzz}^{\text{EZFTC}}$ and $\beta_{\text{HRS}}(-2\omega; \omega, \omega)/\beta_{\text{HRS}}^{\text{EZFTC}}$ with β_{HRS} displaying resonant enhancement for some chromophores at smaller ω values. The computed $\beta_{zzz}/\beta_{zzz}^{\text{EZFTC}}$ is relatively stable for $\omega > 0.2$ bohr⁻¹ for most chromophores.

For both functionals, the computed β_{zzz} and β_{HRS} ratios are in good agreement for large values of ω , but some of the longer chromophores (YLD130, C2, C3, and OLD3) have very large β_{HRS} values at small values of ω , with computed β_{HRS} ratios ranging from 8 to 143. This is presumably due to redshifting of the absorbance closer to 953 nm, the frequency at which resonant enhancement is maximized. Indeed, at this ω range, all four of these molecules have their strongly allowed charge-transfer excitation at ~1.30–1.35 eV = 954–918 nm. The remaining chromophores have higher energy charge-transfer

states at all ω values so do not undergo this resonant enhancement in β_{HRS} . Since this large enhancement occurs in the same ω range as would be predicted with ω -tuning for Koopmans' theorem, this method of "optimizing" ω does not necessarily lead to better predictions of β_{HRS} compared to experiment.

In Figure 10 we plot the difference in the LC-BLYP calculated and experimental β_{HRS} ratio values (experimental

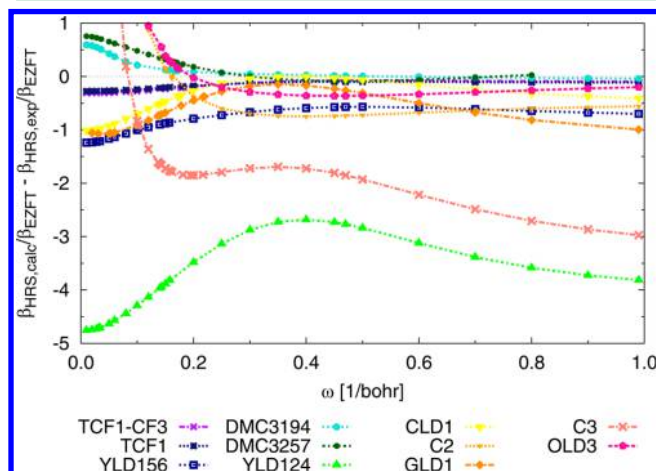


Figure 10. Difference in computed frequency-dependent hyperpolarizability and the experimentally measured $\beta_{\text{HRS}}(-2\omega; \omega, \omega) / \beta_{\text{HRS}}^{\text{EZFTC}}(-2\omega; \omega, \omega)$. No clear trend is observed in ω value and accuracy of computed β_{HRS} . Due to large enhancement of computed β_{HRS} at small ω values for a few of the larger chromophores, ω values below 0.2 bohr⁻¹ may not be suitable for computing this frequency dependent property.

values are given in Table 1, CAM-B3LYP results are given in SI Figure S18). The calculated ratio is generally smaller than the experimental ratio. Outside of the chromophores with large computed ratios at small ω values (OLD3, C3, and C2), the best agreement with the experimental ratio is at approximately $\omega = 0.4$ bohr⁻¹, close to the default value for both functionals. Other than the problem of the computed resonant enhancement for the larger chromophores, there does not appear to be any clear correlation between accuracy and chromophore length or type. The computed β_{HRS} ratios for C3 and YLD124 are underestimated and have the poorest agreement for computed and experimental ratios in the test set. This discrepancy is likely due to the experimental TPF enhancement of the β_{HRS} values at 1907 nm.

Figure 11 summarizes the correlation between the LC-BLYP calculated β_{HRS} ratios and the experimental β_{HRS} ratios at various ω values. β_{HRS} ratios larger than six are not shown on the plot but are included in the least-squares linear fit drawn to guide the eye. All computed β_{HRS} values are given in the SI. The default LC-BLYP ω value of 0.47 bohr⁻¹ gives the most stable behavior. Outside of the two chromophores with experimental resonant enhancement, the correlation with the experimental ratios is quite good. When using the ω value from Koopmans' tuning for ionization potential in vacuum or from the best agreement with λ_{max} in PCM, the calculated β_{HRS} ratios have a bit more scatter, but no computed β_{HRS} ratios are above the experimental maximum ratio of 5.7 (for C3). The smaller ω values from Koopmans' tuning for ionization potential in PCM or from the best agreement with λ_{max} in vacuum lead to the large enhancement for the longer chromophores and also give

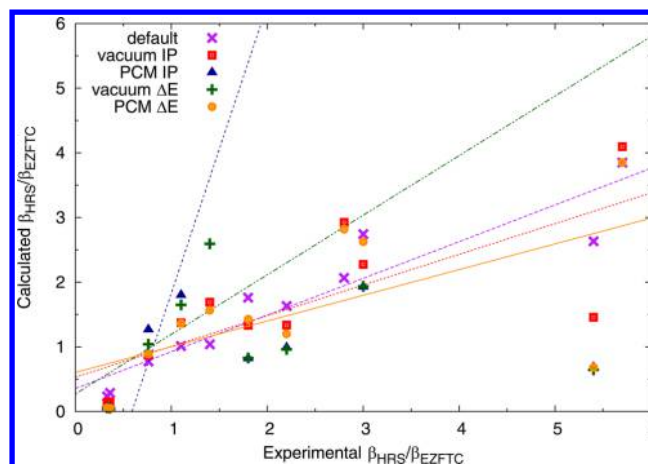


Figure 11. Experimental and LC-BLYP computed $\beta_{\text{HRS}}(-2\omega; \omega, \omega) / \beta_{\text{HRS}}^{\text{EZFTC}}(-2\omega; \omega, \omega)$ correlation plot. The computed $\beta_{\text{HRS}}(-2\omega; \omega, \omega) / \beta_{\text{HRS}}^{\text{EZFTC}}(-2\omega; \omega, \omega)$ values are given for the default ω value of 0.47 bohr⁻¹ (purple x, linear fit of $R^2 = 0.88$), the ω value tuned for agreement with Koopmans' theorem (red ■ for vacuum and blue ▲ for PCM, linear fits of $R^2 = 0.58$ and $R^2 = 0.35$, respectively), and the ω value tuned for agreement with experimental λ_{max} (green + for vacuum and orange ● for PCM, with linear fits of $R^2 = 0.34$ and $R^2 = 0.39$, respectively).

poorer agreement for most of the other chromophores. Overall, due to the unstable behavior of the computed β_{HRS} ratios, these small ω values are not recommended for computing hyperpolarizabilities of NLO chromophores. Although larger ω values that incorporate a substantial amount of exact exchange ($\omega = 0.4$ bohr⁻¹) overestimate the excitation energy compared to λ_{max} , the computed hyperpolarizability ratios are more stable and generally more accurate.

6. CONCLUSIONS

As seen previously, there is a strong correlation between molecular size and the optimum ω value to enforce Koopmans' theorem. Smaller ω values (less exact exchange, more DFT exchange) are needed to enforce this criterion for larger molecules. The presence of a PCM environment shifts the ω -tuning values to $\omega \approx 0.045$ bohr⁻¹ or smaller.

The tuning of ω leads to smaller ω values than the default values, which overall yields more accurate excitation energies. However, we find that ω may be overtuned to a small enough value that the excitation energies go from being consistently overestimated to being underestimated. In contrast to the molecular size trend observed with tuning ω for Koopmans' theorem, better agreement with TDDFT excitation energies and the experimental λ_{max} occurs with larger ω values for larger molecules.

Even with the complication of solvent and resonance effects in comparing our theoretical results to experimental values, it is clear that the smaller ω values predicted for large molecules by tuning ω to enforce Koopmans' theorem do not lead to more accurate hyperpolarizabilities. The most reliable results are obtained with near default ω values of 0.4 bohr⁻¹ for both LC-BLYP and CAM-B3LYP. These results are in agreement with recent work by Champagne and co-workers examining the polarizability α and second hyperpolarizability γ ,⁴⁰ and also with Johnson et al.'s conclusions that large amounts of exchange in hybrid functionals improves accuracy of relative hyperpolarizabilities.⁵⁶ Setting the amount of exchange in a DFT functional to enforce Koopmans' theorem does not offer

improvement in prediction of NLO properties, and we recommend a larger fraction of exact exchange when computing hyperpolarizabilities than would be used for computing excitation energies.

■ ASSOCIATED CONTENT

■ Supporting Information

Cartesian coordinates of all structures in this work. Additional figures and tables as mentioned throughout the text. This material is available free of charge via the Internet at <http://pubs.acs.org>.

■ AUTHOR INFORMATION

Corresponding Author

*Email: cisborn@ucmerced.edu.

Notes

The authors declare no competing financial interest.

■ ACKNOWLEDGMENTS

Work at University of California Merced was supported by UC Merced startup funds. Work at University of Washington was partially supported by the National Science Foundation (STC-MDITR DMR-0120967, DMR-1303080, and DMR-0905686) and the Air Force Office of Scientific Research (FA9550-09-1-0589). The authors thank Prof. Larry Dalton, Dr. Delwin Elder, and Dr. Bruce Eichinger for valuable discussions. We also express special thanks to Dr. Denise Bale for providing experimental data.

■ REFERENCES

- (1) Ding, R.; Baehr-Jones, T.; Liu, Y.; Bojko, R.; Witzens, J.; Huang, S.; Luo, J.; Benight, S.; Sullivan, P.; Fedeli, J. M.; Fournier, M.; Dalton, L.; Jen, A.; Hochberg, M. Demonstration of a Low V- π -L Modulator with GHz Bandwidth Based on Electro-Optic Polymer-Clad Silicon Slot Waveguides. *Opt. Express* **2010**, *18*, 15618–15623.
- (2) Korn, D.; Palmer, R.; Yu, H.; Schindler, P. C.; Alloatti, L.; Baier, M.; Schmogrow, R.; Bogaerts, W.; Selvaraja, S. K.; Lepage, G.; Pantouvaki, M.; Wouters, J. M. D.; Verheyen, P.; Van Campenhout, J.; Chen, B.; Baets, R.; Absil, P.; Dinu, R.; Koos, C.; Freude, W.; Leuthold, J. Silicon–Organic Hybrid (SOH) IQ Modulator Using the Linear Electro-Optic Effect for Transmitting 16QAM at 112 Gbit/s. *Opt. Express* **2013**, *21*, 13219–13227.
- (3) Weimann, C.; Schindler, P. C.; Palmer, R.; Wolf, S.; Bekele, D.; Korn, D.; Pfeifle, J.; Koeber, S.; Schmogrow, R.; Alloatti, L.; Elder, D.; Yu, H.; Bogaerts, W.; Dalton, L. R.; Freude, W.; Leuthold, J.; Koos, C. Silicon–Organic Hybrid (SOH) Frequency Comb Sources for terabit/s Data Transmission. *Opt. Express* **2014**, *22*, 3629–3637.
- (4) Alloatti, L.; Palmer, R.; Diebold, S.; Pahl, K. P.; Chen, B.; Dinu, R.; Fournier, M.; Fedeli, J.-M.; Zwick, T.; Freude, W.; Koos, C.; Leuthold, J. 100 GHz Silicon–Organic Hybrid Modulator. *Light Sci. Appl.* **2014**, *3*, e173.
- (5) Dalton, L. R.; Benight, S. J.; Johnson, L. E.; Knorr, D. B.; Kosilkina, I.; Eichinger, B. E.; Robinson, B. H.; Jen, A. K. Y.; Overney, R. M. Systematic Nanoengineering of Soft Matter Organic Electro-Optic Materials. *Chem. Mater.* **2010**, *23*, 430–445.
- (6) Cyvin, S. J.; Rauch, J. E.; Decius, J. C. Theory of Hyper-Raman Effects (Nonlinear Inelastic Light Scattering): Selection Rules and Depolarization Ratios for the Second-Order Polarizability. *J. Chem. Phys.* **1965**, *43*, 4083–4095.
- (7) Bale, D. H.; Eichinger, B. E.; Liang, W.; Li, X.; Dalton, L. R.; Robinson, B. H.; Reid, P. J. Dielectric Dependence of the First Molecular Hyperpolarizability for Electro-Optic Chromophores. *J. Phys. Chem. B* **2011**, *115*, 3505–3513.
- (8) Akelaitis, A. J. P.; Olbricht, B. C.; Sullivan, P. A.; Liao, Y.; Lee, S. K.; Bale, D. H.; Lao, D. B.; Kaminsky, W.; Eichinger, B. E.; Choi, D. H.; Reid, P. J.; Dalton, L. R. Synthesis and Electro-Optic Properties of Amino-Phenyl-Thienyl Donor Chromophores. *Opt. Mater.* **2008**, *30*, 1504–1513.
- (9) Andzelm, J.; Rinderspacher, B. C.; Rawlett, A.; Dougherty, J.; Baer, R.; Govind, N. Performance of DFT Methods in the Calculation of Optical Spectra of TCF-Chromophores. *J. Chem. Theory Comput.* **2009**, *5*, 2835–2846.
- (10) Benight, S. J.; Johnson, L. E.; Barnes, R.; Olbricht, B. C.; Bale, D. H.; Reid, P. J.; Eichinger, B. E.; Dalton, L. R.; Sullivan, P. A.; Robinson, B. H. Reduced Dimensionality in Organic Electro-Optic Materials: Theory and Defined Order. *J. Phys. Chem. B* **2010**, *114*, 11949–11956.
- (11) Kinnibrugh, T.; Bhattacharjee, S.; Sullivan, P.; Isborn, C.; Robinson, B. H.; Eichinger, B. E. Influence of Isomerization on Nonlinear Optical Properties of Molecules. *J. Phys. Chem. B* **2006**, *110*, 13512–13522.
- (12) Isborn, C. M.; Leclercq, A.; Vila, F. D.; Dalton, L. R.; Brédas, J. L.; Eichinger, B. E.; Robinson, B. H. Comparison of Static First Hyperpolarizabilities Calculated with Various Quantum Mechanical Methods. *J. Phys. Chem. A* **2007**, *111*, 1319–1327.
- (13) Dreuw, A.; Head-Gordon, M. Single-Reference Ab Initio Methods for the Calculation of Excited States of Large Molecules. *Chem. Rev.* **2005**, *105*, 4009–4037.
- (14) Pastirk, I.; Brown, E. J.; Zhang, Q.; Dantus, M. Quantum Control of the Yield of a Chemical Reaction. *J. Chem. Phys.* **1998**, *108*, 4375–4378.
- (15) van Gisbergen, S. J. A.; Schipper, P. R. T.; Gritsenko, O. V.; Baerends, E. J.; Snijders, J. G.; Champagne, B.; Kirtman, B. Electric Field Dependence of the Exchange–Correlation Potential in Molecular Chains. *Phys. Rev. Lett.* **1999**, *83*, 694–697.
- (16) Jacquemin, D.; Perpète, E. A.; Scalmani, G.; Frisch, M. J.; Kobayashi, R.; Adamo, C. Assessment of the efficiency of long-range corrected functionals for some properties of large compounds. *J. Chem. Phys.* **2007**, *126*, 144105.
- (17) Johnson, E. R.; Becke, A. D. A Unified Density-Functional Treatment of Dynamical, Nondynamical, and Dispersion Correlations. II. Thermochemical and Kinetic Benchmarks. *J. Chem. Phys.* **2008**, *128*, 124105.
- (18) Johnson, E. R.; Mori-Sánchez, P.; Cohen, A. J.; Yang, W. Delocalization Errors in Density Functionals and Implications for Main-Group Thermochemistry. *J. Chem. Phys.* **2008**, *129*, 204112.
- (19) Cohen, A. J.; Mori-Sánchez, P.; Yang, W. Fractional Charge Perspective on the Band Gap in Density-Functional Theory. *Phys. Rev. B* **2008**, *77*, 115123.
- (20) Cohen, A. J.; Mori-Sánchez, P.; Yang, W. Insights into Current Limitations of Density Functional Theory. *Science* **2008**, *321*, 792–794.
- (21) Tawada, Y.; Tsuneda, T.; Yanagisawa, S.; Yanai, T.; Hirao, K. A Long-Range-Corrected Time-Dependent Density Functional Theory. *J. Chem. Phys.* **2004**, *120*, 8425–8433.
- (22) Pandey, L.; Doiron, C.; Sears, J. S.; Bredas, J.-L. Lowest Excited States and Optical Absorption Spectra of Donor–Acceptor Copolymers for Organic Photovoltaics: A New Picture Emerging from Tuned Long-Range Corrected Density Functionals. *Phys. Chem. Chem. Phys.* **2012**, *14*, 14243–14248.
- (23) Sekino, H.; Bartlett, R. J. Frequency Dependent Nonlinear Optical Properties of Molecules. *J. Chem. Phys.* **1986**, *85*, 976–989.
- (24) van Gisbergen, S. J. A.; Snijders, J. G.; Baerends, E. J. A Density Functional Theory Study of Frequency-Dependent Polarizabilities and Van der Waals Dispersion Coefficients for Polyatomic Molecules. *J. Chem. Phys.* **1995**, *103*, 9347–9354.
- (25) van Gisbergen, S. J. A.; Snijders, J. G.; Baerends, E. J. Accurate Density Functional Calculations on Frequency-Dependent Hyperpolarizabilities of Small Molecules. *J. Chem. Phys.* **1998**, *109*, 10657–10668.
- (26) Hait Heinze, H.; Della Sala, F.; Görling, A. Efficient Methods to Calculate Dynamic Hyperpolarizability Tensors by Time-Dependent Density-Functional Theory. *J. Chem. Phys.* **2002**, *116*, 9624–9640.
- (27) Vydrov, O. A.; Scuseria, G. E. Assessment of a long-range corrected hybrid functional. *J. Chem. Phys.* **2006**, *125*, 234109.

- (28) Sekino, H.; Maeda, Y.; Kamiya, M.; Hirao, K. Polarizability and Second Hyperpolarizability Evaluation of Long Molecules by the Density Functional Theory with Long-Range Correction. *J. Chem. Phys.* **2007**, *126*, 014107.
- (29) Song, J.-W.; Watson, M. A.; Sekino, H.; Hirao, K. Nonlinear Optical Property Calculations of Polyyenes with Long-Range Corrected Hybrid Exchange-Correlation Functionals. *J. Chem. Phys.* **2008**, *129*, 024117.
- (30) Stein, T.; Kronik, L.; Baer, R. Prediction of Charge-Transfer Excitations in Coumarin-Based Dyes Using a Range-Separated Functional Tuned from First Principles. *J. Chem. Phys.* **2009**, *131*, 2818.
- (31) Baer, R.; Kronik, L.; Stein, T. Reliable Prediction of Charge Transfer Excitations in Molecular Complexes Using Time-Dependent Density Functional Theory. *J. Am. Chem. Soc.* **2009**, *131*, 2818–2820.
- (32) Iikura, H.; Tsuneda, T.; Yanai, T.; Hirao, K. A Long-Range Correction Scheme for Generalized-Gradient-Approximation Exchange Functionals. *J. Chem. Phys.* **2001**, *115*, 3540–3544.
- (33) Vydrov, O. A.; Heyd, J.; Krukau, A. V.; Scuseria, G. E. Importance of Short-Range versus Long-Range Hartree–Fock Exchange for the Performance of Hybrid Density Functionals. *J. Chem. Phys.* **2006**, *125*, 074106.
- (34) Champagne, B. t.; Perpète, E. A.; van Gisbergen, S. J. A.; Baerends, E.-J.; Snijders, J. G.; Soubra-Ghaoui, C.; Robins, K. A.; Kirtman, B. Assessment of Conventional Density Functional Schemes for Computing the Polarizabilities and Hyperpolarizabilities of Conjugated Oligomers: An Ab Initio Investigation of Polyacetylene Chains. *J. Chem. Phys.* **1998**, *109*, 10489–10498.
- (35) Champagne, B.; Perpète, E. A.; Jacquemin, D.; van Gisbergen, S. J. A.; Baerends, E.-J.; Soubra-Ghaoui, C.; Robins, K. A.; Kirtman, B. Assessment of Conventional Density Functional Schemes for Computing the Dipole Moment and (Hyper)polarizabilities of Push–Pull π -Conjugated Systems. *J. Phys. Chem. A* **2000**, *104*, 4755–4763.
- (36) Mori-Sánchez, P.; Wu, Q.; Yang, W. Accurate Polymer Polarizabilities with Exact Exchange Density-Functional Theory. *J. Chem. Phys.* **2003**, *119*, 11001–11004.
- (37) Bulat, F. A.; Toro-Labbé, A.; Champagne, B.; Kirtman, B.; Yang, W. Density-Functional Theory (Hyper)Polarizabilities of Push–Pull π -Conjugated Systems: Treatment of Exact Exchange and Role of Correlation. *J. Chem. Phys.* **2005**, *123*, 014319.
- (38) Limacher, P. A.; Mikkelsen, K. V.; Lüthi, H. P. On the Accurate Calculation of Polarizabilities and Second Hyperpolarizabilities of Polyacetylene Oligomer Chains Using the CAM-B3LYP Density Functional. *J. Chem. Phys.* **2009**, *130*, 194114.
- (39) Bonness, S.; Fukui, H.; Yoneda, K.; Kishi, R.; Champagne, B.; Botek, E.; Nakano, M. Theoretical Investigation on the Second Hyperpolarizabilities of Open-Shell Singlet Systems by Spin-Unrestricted Density Functional Theory with Long-Range Correction: Range Separating Parameter Dependence. *Chem. Phys. Lett.* **2010**, *493*, 195–199.
- (40) Nenon, S.; Champagne, B.; Spassova, M. I. Assessing Long-Range Corrected Functionals with Physically-Adjusted Range-Separated Parameters for Calculating the Polarizability and the Second Hyperpolarizability of Polydiacetylene and Polybutatriene Chains. *Phys. Chem. Chem. Phys.* **2014**, *16*, 7083–7088.
- (41) Krukau, A. V.; Scuseria, G. E.; Perdew, J. P.; Savin, A. Hybrid Functionals with Local Range Separation. *J. Chem. Phys.* **2008**, *129*, 124103.
- (42) Körzdörfer, T.; Sears, J. S.; Sutton, C.; Brédas, J.-L. Long-Range Corrected Hybrid Functionals for π -Conjugated Systems: Dependence of the Range-Separation Parameter on Conjugation Length. *J. Chem. Phys.* **2011**, *135*, 204107.
- (43) Stein, T.; Kronik, L.; Baer, R. Reliable Prediction of Charge Transfer Excitations in Molecular Complexes Using Time-Dependent Density Functional Theory. *J. Am. Chem. Soc.* **2009**, *131*, 2818–2820.
- (44) Stein, T.; Kronik, L.; Baer, R. Prediction of Charge-Transfer Excitations in Coumarin-Based Dyes Using a Range-Separated Functional Tuned from First Principles. *J. Chem. Phys.* **2009**, *131*, 244119–244115.
- (45) Baer, R.; Livshits, E.; Salzner, U. Tuned Range-Separated Hybrids in Density Functional Theory. *Annu. Rev. Phys. Chem.* **2010**, *61*, 85–109.
- (46) Kuritz, N.; Stein, T.; Baer, R.; Kronik, L. Charge-Transfer-Like $\pi \rightarrow \pi^*$ Excitations in Time-Dependent Density Functional Theory: A Conundrum and Its Solution. *J. Chem. Theory Comput.* **2011**, *7*, 2408–2415.
- (47) Karolewski, A.; Stein, T.; Baer, R.; Kümmel, S. Communication: Tailoring the Optical Gap in Light-Harvesting Molecules. *J. Chem. Phys.* **2011**, *134*, 151101.
- (48) Refaely-Abramson, S.; Baer, R.; Kronik, L. Fundamental and Excitation Gaps in Molecules of Relevance for Organic Photovoltaics from an Optimally Tuned Range-Separated Hybrid Functional. *Phys. Rev. B* **2011**, *84*, 075144.
- (49) Kronik, L.; Stein, T.; Refaely-Abramson, S.; Baer, R. Excitation Gaps of Finite-Sized Systems from Optimally Tuned Range-Separated Hybrid Functionals. *J. Chem. Theory Comput.* **2012**, *8*, 1515–1531.
- (50) Sun, H.; Autschbach, J. Influence of the Delocalization Error and Applicability of Optimal Functional Tuning in Density Functional Calculations of Nonlinear Optical Properties of Organic Donor–Acceptor Chromophores. *ChemPhysChem* **2013**, *14*, 2450–2461.
- (51) Karolewski, A.; Kronik, L.; Kümmel, S. Using Optimally Tuned Range Separated Hybrid Functionals in Ground-State Calculations: Consequences and Caveats. *J. Chem. Phys.* **2013**, *138*, -.
- (52) Korzdörfer, T.; Sears, J. S.; Sutton, C.; Bredas, J.-L. Long-Range Corrected Hybrid Functionals for π -Conjugated Systems: Dependence of the Range-Separation Parameter on Conjugation Length. *J. Chem. Phys.* **2011**, *135*, 204107.
- (53) Firestone, K., Frequency-agile hyper-Rayleigh scattering studies of nonlinear optical chromophores, University of Washington, 2005.
- (54) Bale, D. H., Nonlinear Optical Materials Characterization Studies Employing Photostability, Hyper-Rayleigh Scattering, and Electric Field Induced Second Harmonic Generation Techniques, University of Washington, 2008.
- (55) Reis, H. Problems in the Comparison of Theoretical and Experimental Hyperpolarizabilities Revisited. *J. Chem. Phys.* **2006**, *125*, 014506.
- (56) Johnson, L. E.; Dalton, L. R.; Robinson, B. H. Optimizing Calculations of Electronic Excitations and Relative Hyperpolarizabilities of Electrooptic Chromophores. *Acc. Chem. Res.* **2014**, DOI: 10.1021/ar5000727.
- (57) Frisch, M. J.; Trucks, G. W.; Schlegel, H. B.; Scuseria, G. E.; Robb, M. A.; Cheeseman, J. R.; Scalmani, G.; Barone, V.; Mennucci, B.; Petersson, G. A.; Nakatsuji, H.; Caricato, M.; Li, X.; Hratchian, H. P.; Izmaylov, A. F.; Bloino, J.; Zheng, G.; Sonnenberg, J. L.; Hada, M.; Ehara, M.; Toyota, K.; Fukuda, R.; Hasegawa, J.; Ishida, M.; Nakajima, T.; Honda, Y.; Kitao, O.; Nakai, H.; Vreven, T.; Montgomery, J. A., Jr.; Peralta, J. E.; Ogliaro, F.; Bearpark, M. J.; Heyd, J.; Brothers, E. N.; Kudin, K. N.; Staroverov, V. N.; Kobayashi, R.; Normand, J.; Raghavachari, K.; Rendell, A. P.; Burant, J. C.; Iyengar, S. S.; Tomasi, J.; Cossi, M.; Rega, N.; Millam, N. J.; Klene, M.; Knox, J. E.; Cross, J. B.; Bakken, V.; Adamo, C.; Jaramillo, J.; Gomperts, R.; Stratmann, R. E.; Yazyev, O.; Austin, A. J.; Cammi, R.; Pomelli, C.; Ochterski, J. W.; Martin, R. L.; Morokuma, K.; Zakrzewski, V. G.; Voth, G. A.; Salvador, P.; Dannenberg, J. J.; Dapprich, S.; Daniels, A. D.; Farkas, Ö.; Foresman, J. B.; Ortiz, J. V.; Cioslowski, J.; Fox, D. J. *Gaussian 09*; Gaussian, Inc.: Wallingford, CT, 2009.
- (58) Iikura, H.; T, T.; Yanai, T.; Hirao, K. Long-Range Correction Scheme for Generalized-Gradient-Approximation Exchange Functionals. *J. Chem. Phys.* **2001**, *115*, 3540–3544.
- (59) Rohrdanz, M. A.; Herbert, J. M. Simultaneous Benchmarking of Ground- and Excited-State Properties with Long-Range-Corrected Density Functional Theory. *J. Chem. Phys.* **2008**, *129*, 034107–034109.
- (60) Rohrdanz, M. A.; Martins, K. M.; Herbert, J. M. A Long-Range-Corrected Density Functional That Performs Well for Both Ground-State Properties and Time-Dependent Density Functional Theory

Excitation Energies, Including Charge-Transfer Excited States. *J. Chem. Phys.* **2009**, *130*, 054112–054118.

(61) Kamiya, M.; Sekino, H.; Tsuneda, T.; Hirao, K. Nonlinear Optical Property Calculations by the Long-Range-Corrected Coupled-Perturbed Kohn–Sham Method. *J. Chem. Phys.* **2005**, *122*, 234111.

(62) Mori-Sanchez, P.; Cohen, A. J.; Yang, W. Localization and Delocalization Errors in Density Functional Theory and Implications for Band-Gap Prediction. *Phys. Rev. Lett.* **2008**, *100*, 146401.

(63) Refaely-Abramson, S.; Sharifzadeh, S.; Govind, N.; Autschbach, J.; Neaton, J. B.; Baer, R.; Kronik, L. Quasiparticle Spectra from a Nonempirical Optimally Tuned Range-Separated Hybrid Density Functional. *Phys. Rev. Lett.* **2012**, *109*, 226405.

(64) Autschbach, J. Charge-Transfer Excitations and Time-Dependent Density Functional Theory: Problems and Some Proposed Solutions. *ChemPhysChem* **2009**, *10*, 1757–1760.

(65) Subotnik, J. E. Communication: Configuration Interaction Singles Has a Large Systematic Bias against Charge-Transfer States. *J. Chem. Phys.* **2011**, *135*, 071104–071104.